

Article

# Enhancing Segregation Behavior of Impurity by Electromagnetic Stirring in the Solidification Process of Al-30Si Alloy

Qingchuan Zou <sup>1,2,\*</sup>, Ning Han <sup>3</sup>, Zixu Zhang <sup>1</sup>, Jinchuan Jie <sup>2</sup>, Fan Xu <sup>1</sup> and Xizhong An <sup>1</sup>

<sup>1</sup> Key Laboratory for Ecological Metallurgy of Multimetallic Mineral of Ministry of Education, School of Metallurgy, Northeastern University, Shenyang 110819, China; zhangzxxs@163.com (Z.Z.); xufanneu@163.com (F.X.); anxz@mail.neu.edu.cn (X.A.)

<sup>2</sup> School of Material Science and Engineering, Dalian University of Technology, Dalian 116024, China; jiejc@dlut.edu.cn

<sup>3</sup> Department of Chemical Engineering, Curtin University, Perth 6102, Australia; ninghan51@126.com

\* Correspondence: zouqingchuan@mail.neu.edu.cn

Received: 29 December 2019; Accepted: 18 January 2020; Published: 20 January 2020



**Abstract:** Increasing the removal efficiency of impurities during non-equilibrium solidification of hypereutectic Al-Si alloy remains a great challenge for the upgrading of metallurgical silicon (MG-Si) to solar grade Si (SOG-Si). Hence, a manageable method was provided to enhance the segregation behavior of impurities at the interface front of primary Si/Al-Si melt by introducing a rotating magnetic field (RMF) in the present work. Experimental results showed that electromagnetic stirring can improve the removal efficiency of impurities while achieving the separation of primary Si. The apparent segregation coefficients of the major impurities Fe, Ti, Ca, Cu, B and P were reduced to  $7.5 \times 10^{-4}$ ,  $4.6 \times 10^{-3}$ ,  $7.9 \times 10^{-3}$ ,  $3.5 \times 10^{-3}$ , 0.1 and 0.16, respectively, under RMF of 25 mT and cooling rate of 2.5 °C/min. We confirmed that improving the transport driving force of impurities in the growth interface front of primary Si is an effective way to improve the segregation behavior of impurities, which would bring us one step closer to exploiting the economic potential of the Al-Si alloy solidification refining.

**Keywords:** segregation behavior; rotating magnetic field; solidification; microstructure; hypereutectic Al-Si alloy

## 1. Introduction

The accessibility of low-cost solar grade (SOG-Si) is necessary for the increasing use of solar cells. To pursue a better environmental protection processes for silicon purification, scientists have been devoting to refine metallurgical silicon (MG-Si) step by step through the multiple metallurgical technologies, including acid leaching and directional solidification to remove the metallic impurities [1], slag refining to remove B [2] and vacuum refining to remove P [3,4]. In the coupling refining process, the MG-Si has to be heated repeatedly to molten state at each step to ensure the efficient removal of all impurities, which inevitably led to high energy consumption.

In the recent years, the Al-Si alloy solidification refining as a novel metallurgical process, showed significant advantages both production efficiency and economic value because of the low refining temperature as well as the low segregation coefficient of metallic and non-metallic impurities [5–7]. With decreasing of temperature, the primary Si initially precipitated from hypereutectic Al-Si melt where more impurities were rejected into the Al-Si melt under the effect of solute redistribution [6–8], thereby refining the primary Si. However, the removal efficiency of impurities is limited because of the relatively weak segregation behavior of impurities at the interface

of primary Si/Al-Si melt by the non-equilibrium process in Al-Si alloy [9,10]. Much effort has been made to enhance the segregation behavior of impurities in the growth process of primary Si. One idea is to improve the diffusion kinetics of impurities in the growth interface front of primary Si by reducing cooling rate [9,11,12]. Another strategy is to decrease the solubility of impurities in the Al-Si melt by chemically reacting with the other added elements for the target impurity to form the intermetallic compounds [13–18]. Although the removal efficiency of impurities can be improved by reducing cooling rate and chemical reaction, it will spend several weeks to finally remove impurities effectively and increase the risk of secondary pollution largely due to the excessive addition of other elements. Therefore, developing a rapid and simple method to enhance the segregation behavior of impurities during non-equilibrium solidification of Al-Si alloy is still a challenge.

It is well-known that the rotating magnetic field (RMF) has been widely applied in metallurgical field that could realize a contactless melt stirring to significantly influence the solute distribution at the interface front of the solid/liquid in the crystal growing process [19]. In the past, we have attempted to control the growth process of Si crystals by applying RMF during the solidification of hypereutectic Al-Si melt to achieve the in-situ-separation of primary Si [20–24] and systematically revealed its electromagnetic separation mechanism [24]. But the previous investigations focused on the separation control of the primary Si and did not having a deep and systematic research on the segregation behavior of impurities in the growth process of primary Si. If the segregation behavior of impurity elements can be enhanced by applying RMF, the Si refining process will be more practical because it can achieve the electromagnetic separation of primary Si while achieving highly efficient removal of impurities.

Hence, in the present study, we investigated the influence of forced-melt flow generated by RMF on the segregation behavior of impurities at the primary Si/Al-Si melt interface during non-equilibrium solidification of Al-30Si alloy. First, the structure of flow field and the distribution of temperature field were analyzed under electromagnetic stirring. Further, solidification structure was characterized to understand the effect of electromagnetic stirring on the separation of primary Si. On this basis, the enhanced effect of electromagnetic stirring on the segregation behavior of impurities was investigated during the electromagnetic separation of primary Si and the enhancing mechanism was also discussed.

## 2. Materials and Methods

The hypereutectic Al-30 wt.% Si alloy (in weight) was prepared by melting the MG-Si (99.7 wt.%) and commercial Al (99.7 wt.%) in the SiC electric furnace with a high-purity argon atmosphere. Details of chemical compositions are given in Table 1. The Al-30Si melt was maintained to the homogenization treatment at 850 °C for 30 min and then cast into the cylindrical graphite crucible (40 mm inner diameter, 50 mm depth) preheated to 850 °C. The weight of each sample was controlled to be about 60 g. The crucible was pre-placed in an RMF with a frequency of 50 Hz with tunable magnetic intensity, which was induced by a three-phase-three-pole magnetic generator. The thermal insulation material was placed on the periphery of the crucible to introduce the inhomogeneous temperature field into the liquid metal (the solidification is constrained). The fundamental structure of this experimental device is shown in Figure 1. The RMF was switched on when the melt with a cooling rate of 2.5 °C/min was cooled to 855 °C. The magnetic field intensities in this work were 0, 5, 15 and 25 mT, respectively.

**Table 1.** The content of impurity in the raw materials (ppmw).

Element	Fe	Ti	Ca	Cu	B	P
MG-Si	5605	517	33.7	42.9	56	68
Al	1871	26	/	18	4	/
Al-30Si alloy	2991	173	10	25.5	19.6	20.4

Note: Impurity concentration below the test limit.

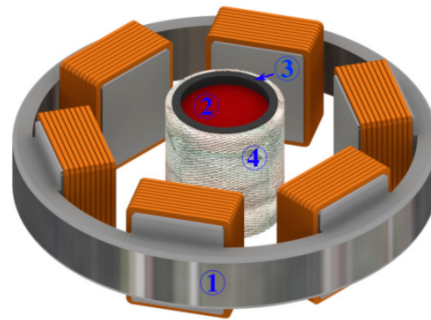


**Figure 1.** Schematic diagram of the experimental device: (1) electromagnetic coil, (2) Al-30Si melt, (3) graphite crucible, (4) thermal insulation material.

The sample was cut into two parts and carefully polished. One part was used for the observation of solidification structure. The microstructure and impurities distribution were measured by Optical Microscope (OM, BX51M, Olympus, Tokyo, Japan) and Electron Probe Microanalyzer (EPMA, EPMA-1600, Shimadzu, Japan). The content of primary Si in the Si-rich layer was measured by X-ray Fluorescence Spectrometry (XRF, XRF-1800, Shimadzu, Japan). Other part was used for the detection of impurities contents. The primary Si was collected through the acid pickling to dissolve the Al matrix in the Si-rich layer, as specifically described in the previous work [23]. The impurities contents in the primary Si were measured by Inductively Coupled Plasma Mass Spectrometry (ICP-MS, NexION 300D, PerkinElmer, Waltham, MA, USA).

### 3. Results and Discussion

#### 3.1. Melt Flow Characteristics and Temperature Field Distribution

This paper will focus on the effect of forced-melt flow generated by RMF on the removal efficiency of impurities during non-equilibrium solidification of Al-30Si melt, which mainly aimed to verify whether the electromagnetic stirring have reinforcement effect to the segregation behavior of impurities. To achieve this goal, we firstly calculated the characteristics of melt flow and the distribution of temperature field using the COMSOL software (No. 5.3, COMSOL Inc., Stockholm, Sweden) and the simulation results are shown in Figure 2. The mathematical models and calculation methods of temperature field and flow field used in this research are consistent with the literature [25,26].

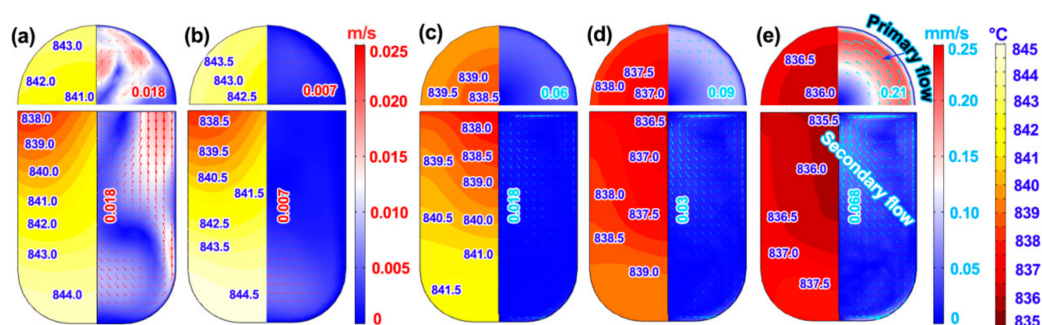


**Figure 2.** Simulation results of temperature field (left side) and flow field (right side) with different conditions: (a) without rotating magnetic field (RMF); (b) 600 mT static magnetic field (SMF); (c) 5 mT RMF; (d) 15 mT RMF and (e) 25 mT RMF.

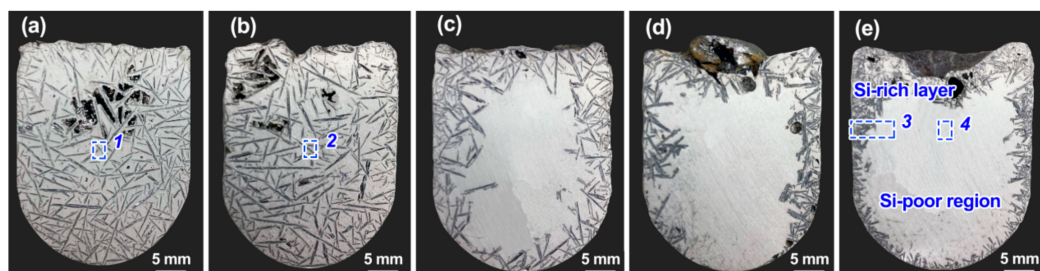
The left side of Figure 2a–e shows the simulation results of distribution of temperature field, when the melt was cooled for 4 min. It can be seen clearly in a bottom-up temperature gradient existed in the vertical section of Al-30Si alloys. This can be explained as the heat preferentially escaped through the top of crucible due to the application of thermal insulation material on the periphery of

the graphite crucible (see Figure 1). To emphasize, the temperature gradient has a tendency of obvious dropping with the application of RMF. The temperature gradient in the vertical section was decreased from 1.5 (without electromagnetic stirring) to 0.5 (RMF of 25 mT) °C/cm.

The simulation results of the characteristics of the flow field are displayed in the right side of Figure 2a–e. From the right side of Figure 2a, the flow pattern in the Al-30Si melt under no RMF was characterized by a relatively strong natural convection, when the maximum flow velocity reaches around 0.018 m/s in the liquid. To determine more fully and strongly the role of melt flow on the segregation behavior of impurities, natural convection was further suppressed by introducing static magnetic field (SMF) with the fundamental structure similar to the experimental device in the literature [27]. It was evident that the melt flow perpendicular to the direction of magnetic field was effectively suppressed, resulting in a significant reduction of maximum flow velocity  $\sim 0.007$  m/s (right side of Figure 2b). To make strong melt convection, RMF was applied to realize a contactless electromagnetic stirring. Under the electromagnetic stirring, an electric current density was induced in the melt according to the induction law and the interaction between the current density and the magnetic field yields a Lorentz force driving the liquid melt in the direction of the magnetic field rotation. This would lead to the formation of a primary flow in the azimuthal direction and a secondary flow in the meridional plane (right sides in Figure 2c–e). The primary flow in the form of a swirl can acutely stir the melt. When magnetic intensity was achieved at 25 mT, the maximum tangent velocity of the primary flow was raised to 0.22 m/s. The pattern of secondary flow presented a symmetric toroidal vortex with a flow direction from the top position along melt axis to the solidification front. Although the secondary flow velocity was relatively weak, which was roughly about 1/3 of the primary flow velocity, it played an important role, which will help to improve the axial transport of the solute atoms and considerably decrease the thermal gradient in the melt.

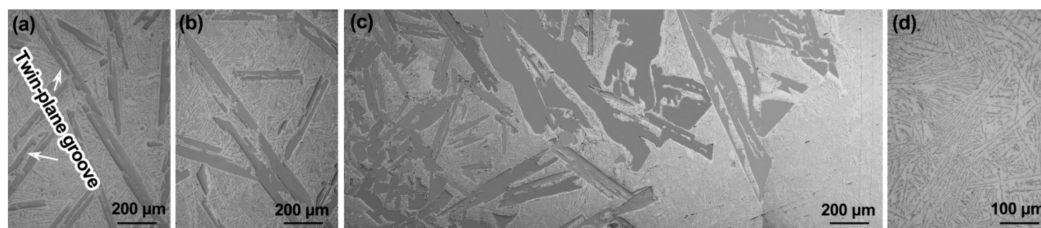
### 3.2. Effect of Electromagnetic Stirring on the Separation of Primary Si

The vertical-section images of Al-30Si alloys solidified with and without RMF are given in Figure 3. In the conventional solidification without RMF, the primary Si (darker color) displayed plate-like morphology and tended to distribute uniformly (Figure 3a). When the SMF was further introduced, the natural convection can be effectively suppressed because of the electromagnetic damping effect [28], leading to more homogeneous distribution of primary Si (Figure 3b). Under the electromagnetic stirring, the primary Si phases were separated and accumulated to the periphery of the ingot during solidification of Al-30Si melt, eventually forming a layer structure with Si-rich outer layer/Si-poor inside region (Figure 3c). In addition, the stronger melt flow might further promote the separation of primary Si from the Al-30Si melt. With the increasing of the magnetic field intensity, the thickness of the Si-rich layer decreased and the density of the primary Si within the layer increased, as shown in Figure 3c–e. When magnetic intensity is achieved to 25 mT, the content of primary Si in the Si-rich layer is measured to be in the range of 65–69 wt.%.



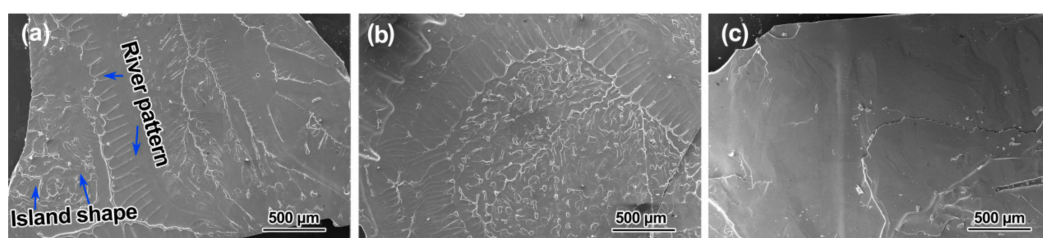
**Figure 3.** Vertical-section images of Al-30Si alloy with different conditions: (a) without rotating magnetic field (RMF), (b) 600 mT static magnetic field (SMF), (c) 5 mT RMF, (d) 15 mT RMF and (e) 25 mT RMF.

Figure 4 shows the microstructures at different positions (as the positions 1–4 marked in Figure 3) of Al-30Si ingots. In the absence of RMF, the primary Si with plate-like was surrounded by the eutectic Al-Si structure (Figure 4a, position 1). The eutectic Al-Si structure is needle-like because the solidification rate exceeded a threshold rate at which the lamella transforms into needles [29]. These primary Si plates are growing parallel to each other with a twin-plane groove in between them. Under the 600 mT SMF, there was no appreciable microstructural change (Figure 4b, position 2). Under the electromagnetic stirring, the formation of Si-rich layer on the periphery of ingot is made up of the large coarse primary Si and a small amount of needle-like eutectic structure (Figure 4c, position 3). The eutectic Al-Si structure can be observed in the middle area of the ingot where no primary Si phase appeared (Figure 4d, position 4). This means that primary Si is close to the threshold of the electromagnetic separation when the Si content of the Al-Si melt reduces to the eutectic composition.



**Figure 4.** Microstructures of different positions in Figure 3: (a) position 1, (b) position 2, (c) position 3 and (d) position 4.

To further reveal the growth dynamic process of primary Si in the electromagnetic separation process, the morphologies of the primary Si phase at the side interface were observed by dissolving the eutectic Al-Si matrix, as shown in Figure 5. In the conventional solidification of Al-30Si alloy (Figure 5a), there are numerous growth traces of the island shape and the river pattern in the side interface of the primary Si caused by the uneven solute accumulation in the solid-liquid interface front [30]. With the natural convection was further suppressed by SMF, the morphologies the island shape and the river pattern become increasingly obvious (Figure 5b). Under the electromagnetic stirring, the structure of the island shape and the river pattern in the side interface of the primary Si disappeared and changed to relatively smooth (Figure 5c). Much of this change can be attributed to promoting transmission of the solute accumulated at the growth interface of primary Si by the electromagnetic stirring.



**Figure 5.** Morphologies of the primary Si at the side interface: (a) without RMF, (b) 600 mT SMF and (c) 25 mT RMF.

### 3.3. Segregation Behavior of Impurities under Electromagnetic Stirring

#### 3.3.1. Effect of Electromagnetic Stirring on the Removal of Impurities

To investigate the influence of electromagnetic stirring on the segregation behavior of the impurities, the distribution of impurities at the interface of primary Si phase/eutectic Al-Si matrix was measured through EPMA and the results are given in Figure 6. It was difficult to remove the nonmetallic impurity B from Si; thus, it was the main object to be investigated in the field of alloy solidification purifying [14–18]. Therefore select B element as research object carried on the EPMA surface and line analysis. For solidification without RMF, a slightly increasing trend can be observed on the intensity

of B K $\alpha$  line from the primary Si phase to the eutectic Al-Si matrix due to the solute redistribution (Figure 6a). Obviously, the application of RMF can significantly change the distribution pattern of the impurity B between the primary Si and the eutectic matrix (Figure 6b). The intensity of B K $\alpha$  line was remarkably higher in the eutectic Al-Si matrix than that in the primary Si because of the enhancing of solute redistribution by RMF. Therefore, it was reasonable to conclude that the electromagnetic stirring can effectively enhance the segregation behavior of impurities in the growth process of primary Si, which will play a prompting role in the removal of impurities.

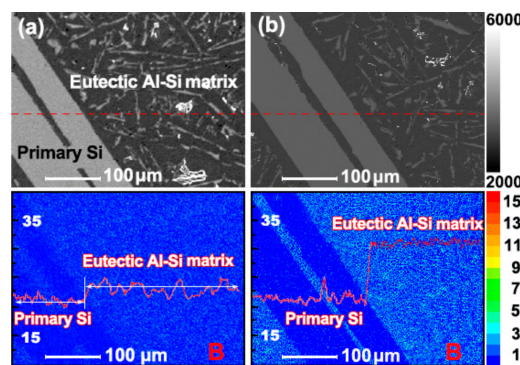


**Figure 6.** The distribution of impurity B at the interface of primary Si/eutectic matrix measured by electron probe microanalyzer (EPMA): (a) without and (b) with RMF of 25 mT.

Figure 7 shows the contents of impurities in the primary Si collected through acid pickling under different solidification conditions. For the solidification without RMF, the contents of impurities Fe, Ti, Ca, Cu, B and P in the primary Si were reduced to 6.4, 2.7, 0.9, 1.1, 7.6 and 9.6 ppmw from 5605, 517, 33.7, 49.2, 56 and 68 ppmw, respectively. With the weak natural convection introduced by SMF, the contents of impurities in the primary Si were slightly increased, and it was not hard to infer that the melt flow has an important role in the removal of impurities during non-equilibrium solidification. Conversely, the forced-melt flow generated further by RMF, the contents of impurities in the primary Si were considerably decreased. When magnetic intensity was achieved to 25 mT, the contents of impurities Fe, Ti, Ca, Cu, B and P were decreased to 2.24, 1.03, 0.13, 0.15, 4.2 and 6.8 ppmw. From Figure 7b, it is proposed the removal fraction of the impurities with different solidification conditions, where the removal fraction was defined from the ratio of the impurity content of primary Si to that of MG-Si [31]. It can be observed that the removal fraction of impurities Fe, Ti, Ca, Cu, B and P were increased by 0.08%, 0.3%, 1.9%, 2.4%, 6.1% and 4.1%, which attained to 99.96%, 99.8%, 99.6%, 99.7%, 92.5% and 90% under RMF of 25 mT than without electromagnetic stirring, respectively. Therefore, the non-equilibrium solidification process of Al-30Si alloy by introducing RMF was a very effective method to improve removal efficiency of impurities from the primary Si.

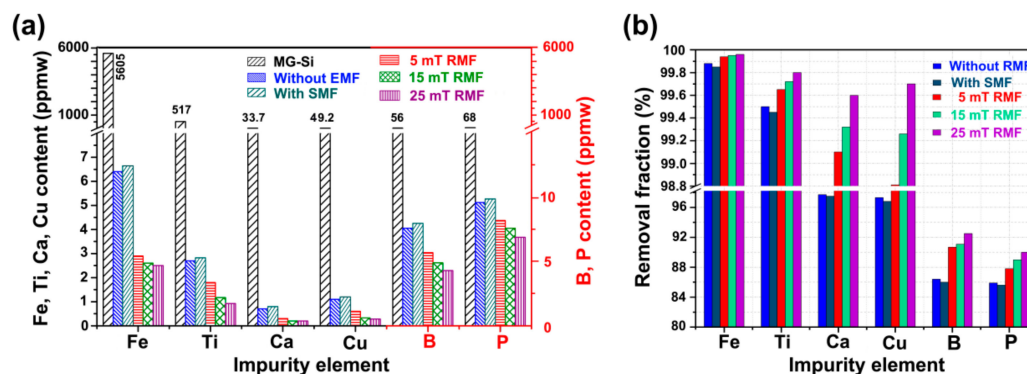


**Figure 7.** Impurities removal from the primary Si in the solidification process of Al-30Si melts under electromagnetic stirring: (a) impurity content, (b) removal fraction.

Although the removal efficiency of impurities can be expressed by the removal fraction, there are still some limitations due to the ignorance of impurity introduction of raw materials Al in the definition of the removal fraction equation. Compared with the removal fraction of the impurities, the apparent segregation coefficient— $k_{i,app}$ —was used to evaluate the segregation behavior of the impurity element more accurately in the non-equilibrium solidification process of Al-Si alloy, which was first proposed by Li [32] and Ban [33], given by:

$$k_{i,app} = \log_{1-f_s} \left( 1 - \frac{\bar{C}_s f_s}{C_0} \right), \quad (1)$$

where  $C_0$  was the initial concentration of impurity in the Al-30Si melt,  $\bar{C}_s$  was the average composition of impurity in the primary Si and  $f_s$  was the fraction of primary Si in the Al-Si melt, which can be calculated according to the Al-Si phase diagram.

According to Equation (1), the apparent segregation coefficients of impurities Fe, Ti, Ca, Cu, B and P were calculated and compared based on the results of this experiment and the data with different solidification conditions from the literature [9,11,14–16,31–38], as shown in Figure 8 and Table 2. It can be determined that the electromagnetic stirring had a reinforcement effect on the segregation behavior of impurities at the interface front of the primary Si/Al-Si melt. The apparent segregation coefficients of impurities Fe, Ti, Ca, Cu, B and P were further decreased from  $1.9 \times 10^{-3}$  to  $7.5 \times 10^{-4}$ ,  $1.4 \times 10^{-2}$  to  $4.6 \times 10^{-3}$ ,  $6.3 \times 10^{-2}$  to  $7.9 \times 10^{-3}$ ,  $3.8 \times 10^{-2}$  to  $3.5 \times 10^{-3}$ , 0.2 to 0.1 and 0.22 to 0.16, respectively, under 25 mT RMF compared to those without electromagnetic stirring. Compared with the traditional technologies, which cover almost all enhancing ideas in this field [9,11,14–16,31–38], it was not difficult to find that the electromagnetic enhancing method proposed in this work has the obvious superiority. The  $k_{i,app}$  obtained in this experiment condition with 25 mT RMF and  $2.5^\circ\text{C}/\text{min}$  cooling rate were considerably lower than that of other experiments. Although  $k_{B,app}$  can be immediately reduced by adding excessive Ti element [14–16], it was no doubt to increase the risk of secondary pollution as the formed  $\text{TiB}_2$  phase ( $\text{Ti} + 2\text{B} \rightarrow \text{TiB}_2$  [39]) would act as the nucleation site for the primary Si. In order to effectively remove B and P, the non-equilibrium solidification process turned into the equilibrium solidification process by unlimited reducing cooling rate [9,11,38], which resulted in the cost of several weeks or even months that the purification efficiency of primary Si would greatly be reduced. Therefore, the segregation behavior of impurities enhanced by electromagnetic stirring in the present study was a very practical technology, because of reducing the dependence on slow-cooling rate and no additives needed without secondary pollution. Particularly, it can achieve the electromagnetic separation of primary Si while enhancing the segregation behavior of impurities and therefore has a strong industrial application potential.

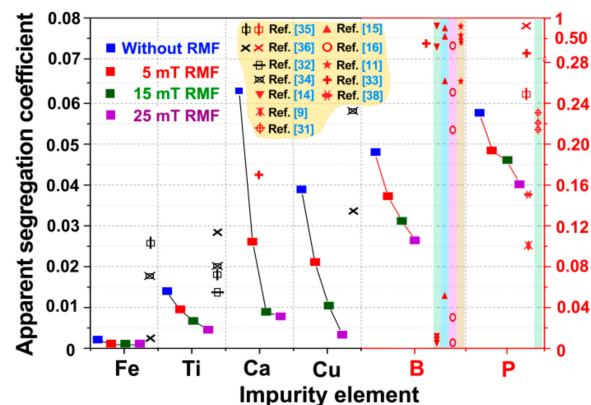


**Figure 8.** The apparent segregation coefficients of impurities in this experiment and comparison with other experiments [9,11,14–16,31–38].

**Table 2.** Apparent segregation coefficients of impurities obtained from the literature.

System	Solidification Condition	Element	$k_{i\text{ app}}$
Al-30Si [34]	Centrifugal solidification	Fe	$1.7 \times 10^{-3}$
		Ti	$2.0 \times 10^{-2}$
		Cu	$5.8 \times 10^{-2}$
Al-45Si [32]	Super gravity solidification 3 °C/min	Ti	$1.3 \times 10^{-2}$
Al-35Si [35]	Super gravity solidification 0.5 °C/min	Fe	$2.6 \times 10^{-2}$
		Ti	$1.8 \times 10^{-2}$
		P	0.25
Al-32Si [36]	Conventional solidification 5 °C/min	Fe	$1.1 \times 10^{-2}$
		Ti	$2.7 \times 10^{-2}$
		Cu	$3.4 \times 10^{-2}$
		P	$0.94$
Al-30Si [14]	Directional solidification, Adding Ti: 0→2000 ppmw 0.5 mm/min	B	0.83 ↓ 0.007
			0.763
Al-42Si [15]	Conventional solidification Adding Ti: 0→575 ppmw 3 °C/min	B	↓ 0.047 0.349
Al-46Si [16]	Adding Ti: 0→3473 ppmw	B	↓ 0.006
Al-30Si [33]	Centrifugal solidification 0.5 °C/min	B	0.45
		P	0.35
Al-30Si [11]	Conventional solidification 1.92→0.033 °C/min	B	0.67 0.26
Al-45Si [37]	Centrifugal solidification 3 °C/min	B	0.135
Al-30Si [9]	Conventional solidification 0.033 °C/min	P	0.01
Al-30Si [31]	Conventional solidification Adding Fe: 0→3000 ppmw 0.03 °C/min		0.23
		P	0.21
			0.24
Al-30Si [38]	Conventional solidification 0.001 °C/min	P	0.14

### 3.3.2. Electromagnetic Enhancing Mechanism

The segregation models of impurities at the primary Si/Al-Si melt interface during non-equilibrium solidification of Al-30Si alloy with and without RMF are shown in Figure 9. In the solidification process without RMF, a bottom-up temperature gradient existed in the axial direction of Al-30Si melt due to the application of thermal insulation material on the periphery of the graphite crucible (left side of Figure 9a). With the cooling time prolonged, the primary Si phases were nucleated and grown along the solidification front until the whole ingot (left side of Figure 9b–d). In the growth process of primary Si, the impurities were excluded to the interface front of the primary Si/Al-Si melt, forming an enriched area (Figure 9c). The impurities in the enriched area were mainly transported in the way of diffusion to the Al-Si melt. The remote transport capacities of impurities were greatly reduced due to the restriction of the non-equilibrium condition. The impurities were easily captured by the growing primary Si that led to the reduction of the removal efficiencies. When solidified under RMF, the temperature gradient was considerably decreased compared to the conventional solidification process, because the secondary flow drives the melt transmission along the axis direction (right side of Figure 9a). The primary Si was pre-nucleated near the top of the melt where the temperature was lower (right side of Figure 9b). Then, the secondary flow carried the bulk Al-Si melt with high Si content to promote the continuous growth of the pre-nucleated primary Si to absorb the Si atoms from the melt, finally resulting in the macro-segregation of primary Si (right side of Figure 9c). When the separation

process reached the limitation at which the Si content in the melt reduced to the eutectic composition, the residual  $\alpha$ -Al melt inside the netlike-region of primary Si can be squeezed out through compression by the primary flow, forming a layer structure with Si-rich outer layer/Si-poor inside region (right side of Figure 9d). The intense melt flow was significantly improved the transport capacity of impurities at the growth interface front of primary Si, which changed from the diffusion controlled to the convection transport. The large number of impurities in the enriched area can be remotely driven from the growth interface front of primary Si into the whole Al-Si melt (Figure 9cII). Thus, a more significant segregation behavior of impurities can be observed for the Al-30Si alloy with RMF compared to that of conventional solidification.

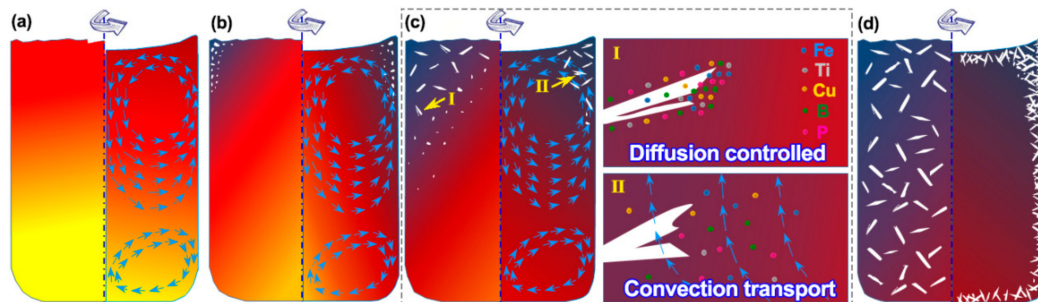


**Figure 9.** Schematic illustration of segregation behavior of impurities in the growth process of primary Si without (left side) and with RMF (right side): (a) the temperature gradient was formed by controlling the heat dissipation of the graphite crucible, (b) the temperature gradient established a low temperature nucleation zone, (c) the primary Si which is the pre-nucleation grew continuously absorbing Si atoms from the remaining liquid metal, (d) the ending of the primary Si growth.

#### 4. Conclusions

In this study, the effect of electromagnetic stirring on the segregation behavior of impurities at the primary Si/Al-Si melt interface during non-equilibrium solidification of Al-30Si melt was comprehensively investigated. The main results are drawn as follows:

1. Numerical simulation results indicate that RMF can notably change the structure of the flow field, which forms a primary flow in the azimuthal direction and a secondary flow in the meridional plane. The maximum tangent velocity of the primary flow can reach 0.22 m/s when magnetic intensity achieved 25 mT, resulting in a stronger revolving stir of Al-30Si melt. The secondary flow presents a symmetric toroidal vortex (flow velocity is about 1/3 of the primary flow velocity), which results in improving the axial transport of the solute atoms and decreasing the thermal gradient of the melt.
2. The nucleation and growth of primary Si can be controlled by the coupling effect of RMF and temperature gradient. The primary Si is separated and accumulated to the periphery of the ingot under the electromagnetic stirring, which forms a layer structure with Si-rich outer layer/Si-poor inside region. With the intensity of RMF increases, the thickness of the Si-rich layer decreases and the density of the primary Si within the layer increases.
3. The enhancing effect of electromagnetic stirring on the segregation behavior of impurity can be confirmed. The apparent segregation coefficients of the major impurities Fe, Ti, Ca, Cu, B and P were reduced to  $7.5 \times 10^{-4}$ ,  $4.6 \times 10^{-3}$ ,  $7.9 \times 10^{-3}$ ,  $3.5 \times 10^{-3}$ , 0.1 and 0.16, respectively, under RMF of 25 mT and cooling rate of 2.5 °C/min. Increasing transport driving force of impurities in front of the growing interface of primary Si could improve the segregation behavior of impurities.

**Author Contributions:** Conceptualization, Q.Z. and J.J.; methodology, Q.Z.; software, Q.Z., F.X. and X.A.; validation, Q.Z. and N.H.; investigation, Q.Z. and Z.Z.; resources, Q.Z. and N.H.; writing—original draft preparation, Q.Z.; writing—review and editing, Q.Z., X.A. and N.H.; funding acquisition, Q.Z. All authors have read and agreed to the published version of the manuscript.

**Funding:** This research was funded by National Natural Science Foundation of China (No. 51901038) and the China Post-doctoral Science Foundation (No. 2019M661112).

**Conflicts of Interest:** The authors declare no conflict of interest.

## References

1. Martorano, M.A.; Neto, J.B.F.; Oliveira, T.S.; Tsubaki, T.O. Refining of metallurgical silicon by directional solidification. *Mater. Sci. Eng. B* **2011**, *176*, 217–226. [[CrossRef](#)]
2. Johnston, M.D.; Barati, M. Distribution of impurity elements in slag-silicon equilibria for oxidative refining of metallurgical silicon for solar cell applications. *Sol. Energy Mater. Sol. Cells* **2010**, *94*, 2085–2090. [[CrossRef](#)]
3. Zheng, S.S.; Abel Engh, T.; Tangstad, M.; Luo, X.T. Separation of phosphorus from silicon by induction vacuum refining. *Sep. Purif. Technol.* **2011**, *82*, 128–137. [[CrossRef](#)]
4. Alemany, C.; Trassy, C.; Pateyron, B.; Li, K.; Delannoy, Y. Refining of metallurgical grade silicon by inductive plasma. *Sol. Energy Mater. Sol. Cells* **2002**, *72*, 41–48. [[CrossRef](#)]
5. Morita, K.; Yoshikawa, T. Thermodynamic evaluation of new metallurgical refining processes for SOG-silicon production. *Trans. Nonferrous Met. Soc. China* **2011**, *21*, 685–690. [[CrossRef](#)]
6. Yoshikawa, T.; Morita, K. Refining of silicon during its solidification from a Si-Al melt. *J. Cryst. Growth* **2009**, *311*, 776–779. [[CrossRef](#)]
7. Yoshikawa, T.; Morita, K. Influence of growth velocity on the separation of primary silicon in solidified Al-Si hypereutectic alloy driven by a pulsed electric current. *Metals* **2017**, *7*, 184.
8. Yoshikawa, T.; Morita, K. Removal of phosphorus by the solidification refining with Si-Al melts. *Sci. Technol. Adv. Mat.* **2003**, *4*, 531–537. [[CrossRef](#)]
9. Ban, B.Y.; Bai, X.L.; Li, J.W.; Chen, J.; Dai, S.Y. Effect of kinetics on P removal by Al-Si solvent refining at low solidification temperature. *J. Alloys Compd.* **2016**, *685*, 604–609. [[CrossRef](#)]
10. Wolczynski, W.; Ivanova, A.A.; Kwapisinski, P.; Olejnik, E. Structural transformations versus hard particles motion in the brass ingots. *Arch. Metall. Mater.* **2017**, *62*, 2461–2467. [[CrossRef](#)]
11. Li, Y.L.; Chen, J.; Ban, B.Y.; Zhang, T.T.; Dai, S.Y. Effect of cooling rate on boron removal and solidification behavior of Al-Si alloy. *High Temp. Mater. Proc.* **2015**, *34*, 43–49. [[CrossRef](#)]
12. Bai, X.L.; Ban, B.Y.; Li, J.W.; Peng, Z.J.; Chen, J. Distribution behavior of B and P during Al-Si melt directional solidification with open-ended crucible. *High Temp. Mater. Proc.* **2017**, *37*, 1–8. [[CrossRef](#)]
13. Yoshikawa, T.; Arimura, K.; Morita, K. Boron removal by titanium addition in solidification refining of silicon with Si-Al melt. *Metall. Mater. Trans. B* **2005**, *36*, 837–843. [[CrossRef](#)]
14. Bai, X.L.; Ban, B.Y.; Li, J.W.; Fu, Z.Q.; Peng, Z.J.; Wang, C.B.; Chen, J. Effect of Ti addition on B removal during silicon refining in Al-30%Si alloy directional solidification. *Sep. Purif. Technol.* **2017**, *174*, 345–351. [[CrossRef](#)]
15. Ban, B.Y.; Li, J.W.; Bai, X.L.; He, Q.X.; Chen, J.; Dai, S.Y. Mechanism of B removal by solvent refining of silicon in Al-Si melt with Ti addition. *J. Alloys Compd.* **2016**, *672*, 489–496. [[CrossRef](#)]
16. Lei, Y.; Sun, L.E.; Ma, W.H.; Wei, K.X.; Morita, K. Enhancing B removal from Si with small amounts of Ti in electromagnetic solidification refining with Al-Si alloy. *J. Alloys Compd.* **2016**, *666*, 406–411. [[CrossRef](#)]
17. Lei, Y.; Ma, W.H.; Sun, L.E.; Wu, J.J.; Morita, K. Effects of small amounts of transition metals on boron removal during electromagnetic solidification purification of silicon with Al-Si solvent. *Sep. Purif. Technol.* **2016**, *162*, 20–23. [[CrossRef](#)]
18. Lei, Y.; Ma, W.H.; Sun, L.E.; Wu, J.J.; Dai, Y.N.; Morita, K. Removal of B from Si by Hf addition during Al-Si solvent refining process. *Sci. Technol. Adv. Mat.* **2016**, *17*, 12–19. [[CrossRef](#)]
19. Stiller, J.; Fraña, K.; Cramer, A. Transitional and weakly turbulent flow in a rotating magnetic field. *Phys. Fluids* **2006**, *18*, 074105. [[CrossRef](#)]
20. Zou, Q.C.; Jie, J.C.; Sun, J.L.; Wang, T.M.; Cao, Z.Q.; Li, T.J. Effect of Si content on separation and purification of the primary Si phase from hypereutectic Al-Si alloy using rotating magnetic field. *Sep. Purif. Technol.* **2015**, *142*, 101–107. [[CrossRef](#)]
21. Zou, Q.C.; Jie, J.C.; Liu, S.C.; Sun, X.L.; Li, T.J.; Wang, T.M.; Yin, G.M. Effect of Sn addition on the separation and purification of primary Si from solidification of Al-30Si melt under electromagnetic stirring. *J. Alloys Compd.* **2017**, *725*, 1264–1271. [[CrossRef](#)]
22. Zou, Q.C.; Jie, J.C.; Wang, T.M.; Li, T.J. An efficient method to purify metallurgical grade Si by electromagnetic semi-continuous casting of Al-30Si melt. *Mater. Lett.* **2016**, *185*, 59–62. [[CrossRef](#)]

23. Zou, Q.C.; Jie, J.C.; Liu, S.C.; Wang, T.M.; Yin, G.M.; Li, T.J. Effect of traveling magnetic field on separation and purification of Si from Al-Si melt during solidification. *J. Cryst. Growth* **2015**, *429*, 68–73. [[CrossRef](#)]
24. Jie, J.C.; Zou, Q.C.; Sun, J.L.; Lu, Y.P.; Wang, T.M.; Li, T.J. Separation mechanism of primary Si phase from the hypereutectic Al-Si alloy using rotating magnetic field during solidification. *Acta Mater.* **2014**, *72*, 57–66. [[CrossRef](#)]
25. Nikrityuk, P.A.; Eckert, K.; Grundmann, R. A numerical study of unidirectional solidification of a binary metal alloy under influence of a rotating magnetic field. *Int. J. Heat Mass Transf.* **2006**, *49*, 1501–1515. [[CrossRef](#)]
26. Nikrityuka, P.A. Spin-up of a liquid metal flow driven by a rotating magnetic field in a finite cylinder: A numerical and an analytical study. *Phys. Fluids* **2005**, *17*, 067101. [[CrossRef](#)]
27. Shen, Z.; Zhou, B.F.; Zhong, Y.B.; Zheng, T.X.; Ren, W.L.; Lei, Z.S.; Ren, Z.M. Revealing influence mechanism of a transverse static magnetic field on the refinement of primary dendrite spacing during directional solidification. *J. Cryst. Growth* **2019**, *517*, 54–58. [[CrossRef](#)]
28. Utech, H.P.; Flemings, M.C. Elimination of solute banding in indium antimonide crystals by growth in a magnetic field. *J. Appl. Phys.* **1966**, *37*, 2021–2024. [[CrossRef](#)]
29. Wolczynski, W. Lamella/rod transformation as described by the criterion of minimum entropy production. *Int. J. Thermodyn.* **2010**, *13*, 35–42.
30. Yan, P.Y.; Mao, W.M.; Fan, J.; Wang, B.K. Simultaneous refinement of primary Si and modification of eutectic Si in A390 alloy assisting by Sr-modifier and serpentine pouring channel process. *Materials* **2019**, *12*, 3109. [[CrossRef](#)]
31. Li, Y.L.; Jian, C.; Dai, S.Y. Effect of iron addition (up to 10,000 ppmw) on silicon purification during Al-Si solvent refining. *J. Cryst. Growth* **2016**, *453*, 49–53. [[CrossRef](#)]
32. Li, J.W.; Guo, Z.C. Thermodynamic evaluation of segregation behaviors of metallic impurities in metallurgical grade silicon during Al-Si solvent refining process. *J. Cryst. Growth* **2014**, *394*, 18–23. [[CrossRef](#)]
33. Ban, B.Y.; Li, Y.L.; Zuo, Q.X.; Zhang, T.T.; Chen, J.; Dai, S.Y. Refining of metallurgical grade Si by solidification of Al-Si melt under electromagnetic stirring. *J. Mater. Process. Technol.* **2015**, *222*, 142–147. [[CrossRef](#)]
34. Seo, K.H.; Jeon, J.B.; Youn, J.W.; Kim, S.J.; Kim, K.Y. Recycling of Al-Si die casting scraps for solar Si feedstock. *J. Cryst. Growth* **2016**, *422*, 1–7. [[CrossRef](#)]
35. Li, J.W.; Guo, Z.C.; Tang, H.Q.; Wang, Z.; Sun, S.T. Si purification by solidification of Al-Si melt with super gravity. *Trans. Nonferrous Met. Soc. China* **2012**, *22*, 958–963. [[CrossRef](#)]
36. Tang, T.Y.; Lai, H.X.; Sheng, Z.L.; Gan, C.H.; Xing, P.F.; Luo, X.T. Effect of tin addition on the distribution of phosphorus and metallic impurities in Si-Al alloys. *J. Cryst. Growth* **2016**, *453*, 13–19. [[CrossRef](#)]
37. Li, J.W.; Guo, Z.C.; Tang, H.Q.; Li, J.C. Removal of impurities from metallurgical grade silicon by liquation refining method. *High Temp. Mater. Proc.* **2013**, *32*, 503–510. [[CrossRef](#)]
38. Li, Y.L.; Ban, B.Y.; Li, J.W.; Zhang, T.T.; Bai, X.L.; Chen, J.; Dai, S.Y. Effect of cooling rate on phosphorus removal during Al-Si solvent refining. *Metall. Mater. Trans. B* **2015**, *46*, 542–544. [[CrossRef](#)]
39. Chen, Z.N.; Kang, H.J.; Fan, G.H.; Li, J.H.; Lu, Y.P.; Jie, J.C.; Zhang, Y.B.; Li, T.J.; Jian, X.G.; Wang, T.M. Grain refinement of hypoeutectic Al-Si alloys with B. *Acta Mater.* **2016**, *120*, 168–178. [[CrossRef](#)]

